Research Article

Geological Core Ground Reorientation Technology Application on In Situ Stress Measurement of an Over-Kilometer-Deep Shaft

Chunde Ma,[1,2] Xibing Li,[1] Jiangzhan Chen ⬤,[1] Yanan Zhou,[1] and Sen Gao[1]

[1]*School of Resources and Safety Engineering, Central South University, Changsha, Hunan 410083, China*
[2]*Center for Advanced Study, Central South University, Changsha, Hunan 410083, China*

Correspondence should be addressed to Jiangzhan Chen; jiangzhanchen@csu.edu.cn

As mining progresses to depth, engineering activities face the extreme challenge of high in situ stress. To efficiently measure the deep in situ stress before engineering excavation, an innovative deep in situ stress measurement method capable of the geological core ground reorientation technology and acoustic emission (AE) technology was proposed. With this method, nonorientation geological cores collected from the thousand-meter-deep borehole were reoriented based on the spatial spherical geometry model and borehole bending measurement principle. The distribution of deep in situ stress of an over-kilometer-deep shaft in the Xiangxi gold mine was investigated with real-time synchronized MTS 815 material testing machine and PCI-II AE instrument. The results show that the in situ stress changes from being dominated by horizontal stress to being dominated by vertical stress with depth. The horizontal maximum principal stress and vertical stress gradually increase with depth and reach a high-stress level (greater than 25 MPa) at a depth of 1000 m. The direction of the maximum principal stress is near the north. Meanwhile, to analyze the accuracy of the measured in situ stress comparatively, the stress relief measurements were performed at a depth of 655–958 m in the mine, using the Swedish LUT rock triaxial in situ stress measurement system. The distribution of deep in situ stress obtained by the stress relief method agrees well with that by the AE method, which proves the reliability of the AE in situ stress testing method based on the geological core ground reorientation technology.

1. Introduction

In situ stress is the internal stress in rock mass in the crust. It is the fundamental force that causes the deformation and failure of underground excavation structures such as mines, tunnels, and chambers [1–3]. In mining engineering, the influence of in situ stress increases with the increase in burial depth of the mine year by year [4–7]. The high in situ stress in depth causes an increased risk of rockburst and seismicity and brings significant challenges to the excavation and support of engineering structures [8–11]. Therefore, it is a necessary prerequisite to conduct measurement and understand the distribution of in situ stress in the crust for the scientific design and excavation of deep engineering structures [12–15].

At present, the investigation and development of deep in situ stress measurement technology have attracted increasing attention of many scholars and engineers [16–19]. Compared with the shallow subsurface, the complex geological conditions and limited measurement space in depth make it challenging to measure in situ stress accurately. Correspondingly, there are only a few theories and methods available for deep (over one kilometer or up to a few kilometers' depth) in situ stress measurement [1, 12, 20–22]. The theories and methods that are easy to operate, cost-effective, and readily available for large-scale application are almost a blank.

For the in situ stress measurement of rock mass with considerable depth, the existing mainstream methods, such as stress relief, hydraulic fracturing, and acoustic emission (AE), have been applied in the measurement engineering, but there are some limitations in the practical applications. The stress relief method is a proven quantitative in situ stress measurement technique. However, the measurement process requires

the measurement operator and equipment to reach the deep measurement position [1, 21], which significantly limits the operability of this method in deep narrow space. Besides, the uncertainty in the constitutive behavior of deep rock affects the accuracy of the stress relief method. The hydraulic fracturing method is an effective method to measure deep in situ stress but is still essentially a plane stress measurement technique. To obtain the actual three-dimensional in situ stress distribution in depth, it is necessary to perform hydraulic fracturing measurement in more than three intersection boreholes [23, 24]. Although a single borehole hydraulic fracturing method has been developed in recent years [25], the operation is complex, and many environmental conditions limit the success rate and accuracy. Compared with the former two methods, the acoustic emission (AE) method can be carried out in the laboratory with more stable test conditions and lower test costs [19, 26]. However, this method requires special oriented coring tools to drill the orientation core in the borehole before testing. The high-cost, low-efficiency, and time-consuming oriented coring processes prevent the AE method from being effectively promoted [27]. Currently, some core orientation methods have been developed, such as paleomagnetic orientation, borehole TV, and stratigraphic scanning orientation, whereas they all have some limitations in actual engineering applications [28, 29]. Therefore, oriented coring or core orientation in the large-depth rock mass is still a very laborious task.

In this paper, a new method for the ground reorientation of the geological core is proposed. The geological core ground reorientation technology replaces the cumbersome operation of core orientation in the large-depth borehole, making the AE method an ideal technology for large-depth in situ stress measurement.

2. Geological Core Ground Reorientation Technology

2.1. Theory of Geological Core Ground Reorientation Technology

2.1.1. Precondition of Geological Core Reorientation. During the process of deep drilling and coring production, bending of the borehole will occur without exception due to geological and technological factors. Moreover, the axis of the core is always in line with that of the borehole under normal drilling conditions. Therefore, it is possible to characterize the bending state of the core column using the borehole incline-measure data. The geological core ground reorientation is based on the above conditions and uses known incline-measure data to calculate the other additional incline-measure related data. Further, the continuously linked inclinometry is carried out in reverse with an inclinometer calibration stage to reorientate the in situ orientation of the core.

2.1.2. Spatial Spherical Geometry Model of Incline-Measure Data. Figure 1 shows the spatial spherical coordinates of the upper (A) and lower (B) measuring points of single incline-measure data. PP' is the upright diameter of the sphere,

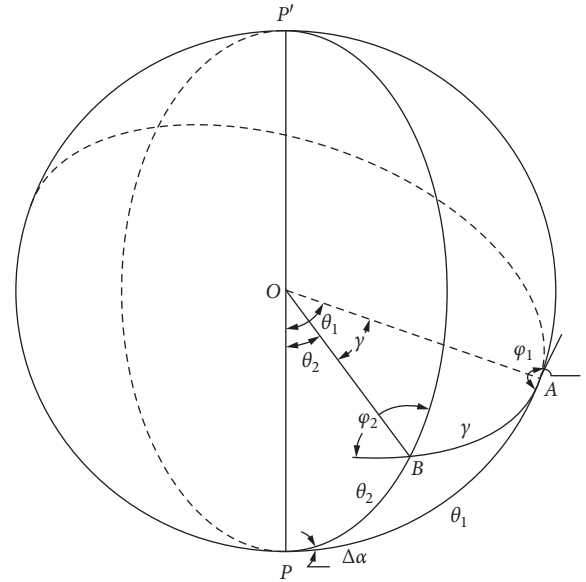FIGURE 1: Mapping of incline-measure data in a spatial spherical coordinate.

$OP'AP$ and OP'BP are two large upright circles, and OAB is the large inclined circle. OA and OB are the adjacent upper and lower measuring points of the borehole, θ_1 and θ_2 are zenith angles, γ is the total bending angle, and $\Delta\alpha$ is the change value of azimuth between two large upright circles. φ_1 and φ_2, angles between the two upright large circles and the large inclined circle, are the special values of the end angle of the upper (A) and lower (B) measuring points. Thus, the three sides of the spherical triangle ABP are θ_1, θ_2, and γ, and the three angles are $\pi-\varphi_1$, φ_2, and $\Delta\alpha$. For the above parameters, if any three parameters are known, the other three parameters can be calculated according to the spherical triangle correlation.

2.1.3. Geological Core Ground Reorientation Based on an Inverse Process of Continuously Linked Inclinometry. Continuously linked inclinometry is the use of measuring tools to obtain the zenith angle θ_i, zenith angle θ_{i+1}, end angle φ_i, and end angle φ_{i+1} ($\Delta\varphi = \varphi_{i+1} - \varphi_i$) at the upper and lower end of a measuring section of the borehole. After that, the change value of azimuth $\Delta\alpha$ can be calculated to orient the borehole. The inverse process is to calculate the total bending angle γ, end angle φ_1, and end angle φ_2 under the condition that the zenith angle θ_1, zenith angle θ_2, and azimuth change value $\Delta\alpha$ are known. Further, $\pi-\varphi_1$, φ_2, γ, and the other three parameters (θ_1, θ_2, and $\Delta\alpha$) constitute the unique spherical triangle, as shown in Figure 1. According to the above six parameters (φ_1, φ_2, γ, θ_1, θ_2, and $\Delta\alpha$), the in situ spatial posture of the core is restored using an inclinometer calibration stage.

2.2. Procedure of Geological Core Ground Reorientation Technology. Ground reorientation method of the non-orientation core includes the following steps.

(1) Sampling: the fresh geological cores are collected from the drilling site or geological core library. The geological cores need to ensure that the structure is complete, the length-diameter ratio is greater than 5, the upper end is marked, and the sampling depth is precise. The cores whose fractures coincide with each other should be collected as much as possible to help improve the measurement accuracy.

(2) Collection and analysis of incline-measure data: the incline-measure data of the borehole are collected, including the borehole depth, zenith angle, and azimuth angle. Based on the borehole depth, the upper and lower ends of each core sample are matched with the corresponding zenith angles θ and azimuth angle α. If the sampling point is between the adjacent incline-measure points, the zenith angles and azimuth angles of the upper and lower ends of each core sample can be obtained by mathematical interpolation or stereographic projection-spherical triangle method. Further, φ_1, φ_2, and γ of the upper and lower ends of each core sample can be calculated by spherical trigonometric formula as follows:

$$\begin{cases} ctg\varphi_2 = -\cos\theta_2 \cdot ctg\Delta\alpha + ctg\theta_1 \cdot \sin\theta_2 \cdot \csc\Delta\alpha, \\ ctg(\pi - \varphi_1) = -\cos\theta_1 \cdot ctg\Delta\alpha + ctg\theta_2 \cdot \sin\theta_1 \cdot \csc\Delta\alpha, \\ \cos\gamma = \cos\theta_1 \cdot \cos\theta_2 + \sin\theta_1 \cdot \sin\theta_2\cos\Delta\alpha. \end{cases}$$

$$(1)$$

(3) Reverse measurement and reorientation: the inclinometer calibration stage, inclinometer shell, core coaxial fixture, and small-diameter inclinometer or fixed-plate inclinometer are used together to restore the spatial posture of nonorientation cores. The small-diameter inclinometer or fixed-plate inclinometer is fixed in inclinometer calibration stage, and the upper section of the core is clamped into the core coaxial fixture first. The inclinometer calibration stage is then adjusted to calibrate the zenith angle and azimuth angle of the upper section of the core. After that, the core coaxial fixture is released, and the core and inclinometer are rotated axially until the end angles of the upper and lower section coincide with the calculated values. Further, the spatial posture of the core is locked, and a generatrix line is marked on the core in the vertical direction (the direction indicating the weight of the inclinometer). The generatrix line is the intersection line of the plane where the total bending angle is located and the core column surface. Finally, a horizontal ellipse is marked on the core column surface, and the north (N) direction is also marked on the horizontal ellipse according to the azimuth angle, as shown in Figure 2.

3. In Situ Stress Measurement after Reorientation

3.1. Sample Processing for AE Test.
All the geological cores of in situ stress measurement were collected from the ZK2
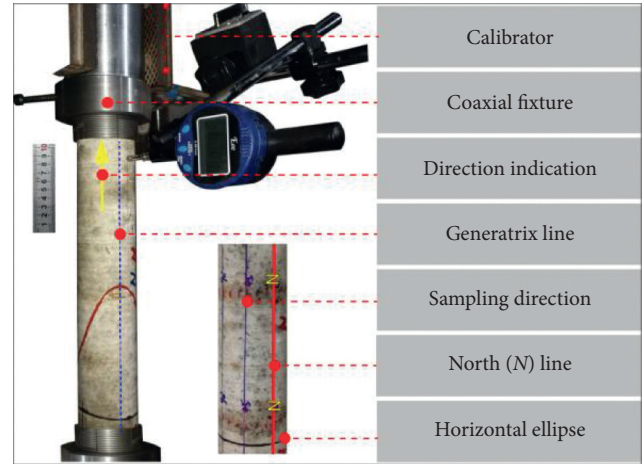

Figure 2: Reorientation of the nonorientation core.

geological borehole (the maximum borehole depth of 1040 m) in the Xiangxi gold mine of Hunan Province, China, as shown in Figure 3. To grasp the distribution of in situ stress with depth and highlight the distribution of in situ stress in deep areas, geological cores with a diameter of 65 mm were taken from 200, 400, 600, 800, 900, and 1000 m depths of the borehole, respectively.

After the cores were reoriented accurately, the cylindrical samples for AE test were drilled from four directions of the cores, as shown in Figure 4. Three to five samples were drilled in the vertical direction, and its role was to determine the vertical stress according to the Kaiser point. Three to five samples were drilled, respectively, from three directions at 0° (N), 45°, and 90° on the horizontal ellipse plane of the core, to determine the direction and value of the horizontal maximum principal stress and the horizontal minimum principal stress according to the Kaiser points. To ensure the reliability of test results, samples were drilled and cut to a diameter of 25 mm and a height of 50 mm. Both ends of each sample were carefully polished on the diamond grinding table.

3.2. Test Equipment.
The loading instrument used in the test is American MTS 815 servocontrolled rigid material testing machine with the 793 control system, as shown in Figure 5(a). The testing machine has a maximum load of 2600 kN and can precisely control load, displacement, and strain in a variety of modes. Besides, the test system is equipped with PCI-II multichannel AE instrument [30, 31]. Before the test, the above two instruments are modified synchronously, and the load data of the MTS 815 testing machine are introduced into the AE instrument as external parameter signals, as shown in Figure 5(b). Thus the AE events and the corresponding stress values can be simultaneously collected by the AE instrument at a megahertz-level rate, which improves the accuracy of judgment of the Kaiser point.

3.3. Test Methods and Parameter Settings.
The purpose of the AE test is to stimulate AE signals of rock samples by uniaxial compressive loading and then identify and
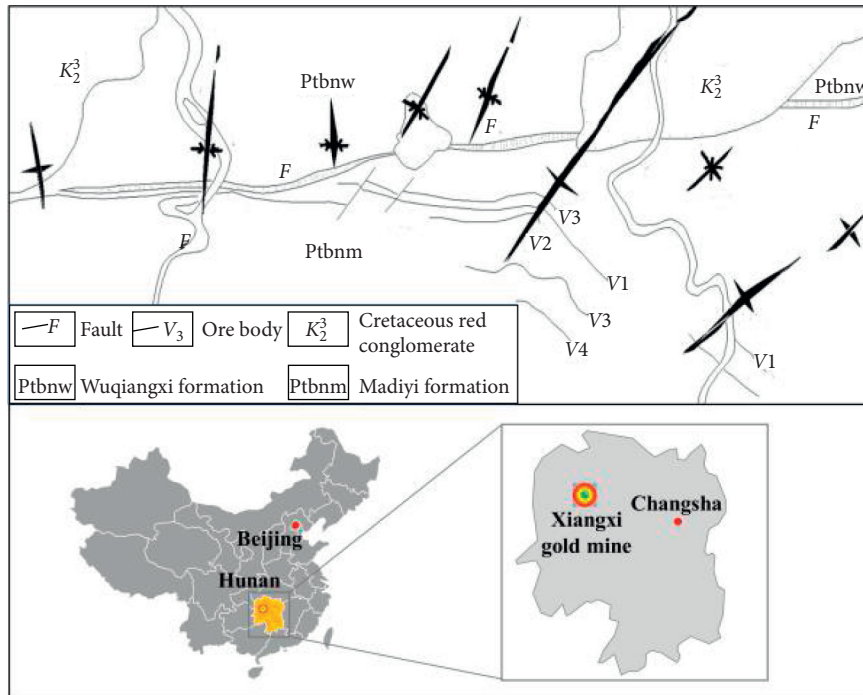
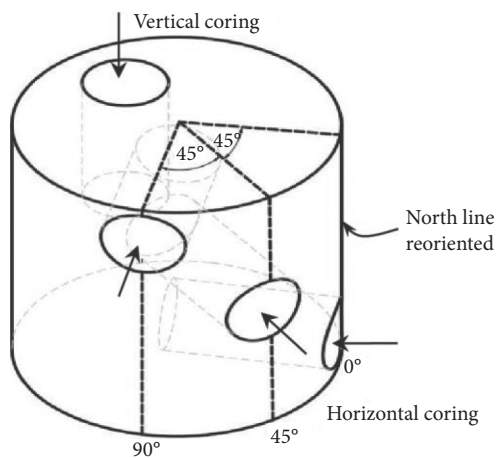FIGURE 3: Schematic diagram of the structural geology of Xiangxi gold mine.

FIGURE 4: Four-direction sampling of reorientation cores.

determine the Kaiser points corresponding to in situ stress in AE signals. The displacement rate control mode of MTS testing machine was adopted in the test. The loading speed was set at 0.1 mm/min under the graded cyclic loading state. The first-level stress of cyclic loading should be higher than the predicted in situ stress. Moreover, the dual-channel data acquisition mode of the AE instrument was adopted and the two AE probes (resonance frequency of 20–400 kHz) were placed on the opposite side of the sample. The preamplifier of the AE instrument was set to 40 dB, the noise threshold was 40 dB, and the AE sampling

frequency is 1 MHz. In addition, the coupling agent was applied to the contact surface between the test sample and the AE probe, to ensure that the AE signal can be well received; a thin layer of petrolatum was applied at the interface between the press head and the test sample, to reduce the effect of end noise on the AE test results.

Figure 5(c) shows that both the loading value and the AE signals are collected simultaneously on the same time axis during the loading process. The mutation point of AE signal is well matched to the external load for the identification of Kaiser point and the corresponding stress.

4. Results and Discussion

4.1. Calculation and Analysis of In Situ Stress. According to the above AE test method, the initial Kaiser points of samples drilling from four directions are determined, and their corresponding loads are found, as shown in Figure 6. To ensure the validity of the test results, a minimum of 15 samples per depth were taken for AE test, and the average value of the results after removing astronomical deviation data is taken as the Kaiser stress, as shown in Table 1.

The Kaiser stress in the vertical direction in Table 1 is regarded as the vertical stress corresponding to the buried depth. The three Kaiser stresses in the horizontal direction (0°, 45°, and 90°) in Table 1 are taken into the plane stress calculation equation (2) to calculate the magnitude and direction of the horizontal maximum and horizontal minimum principal stress [29], as shown in Table 2.
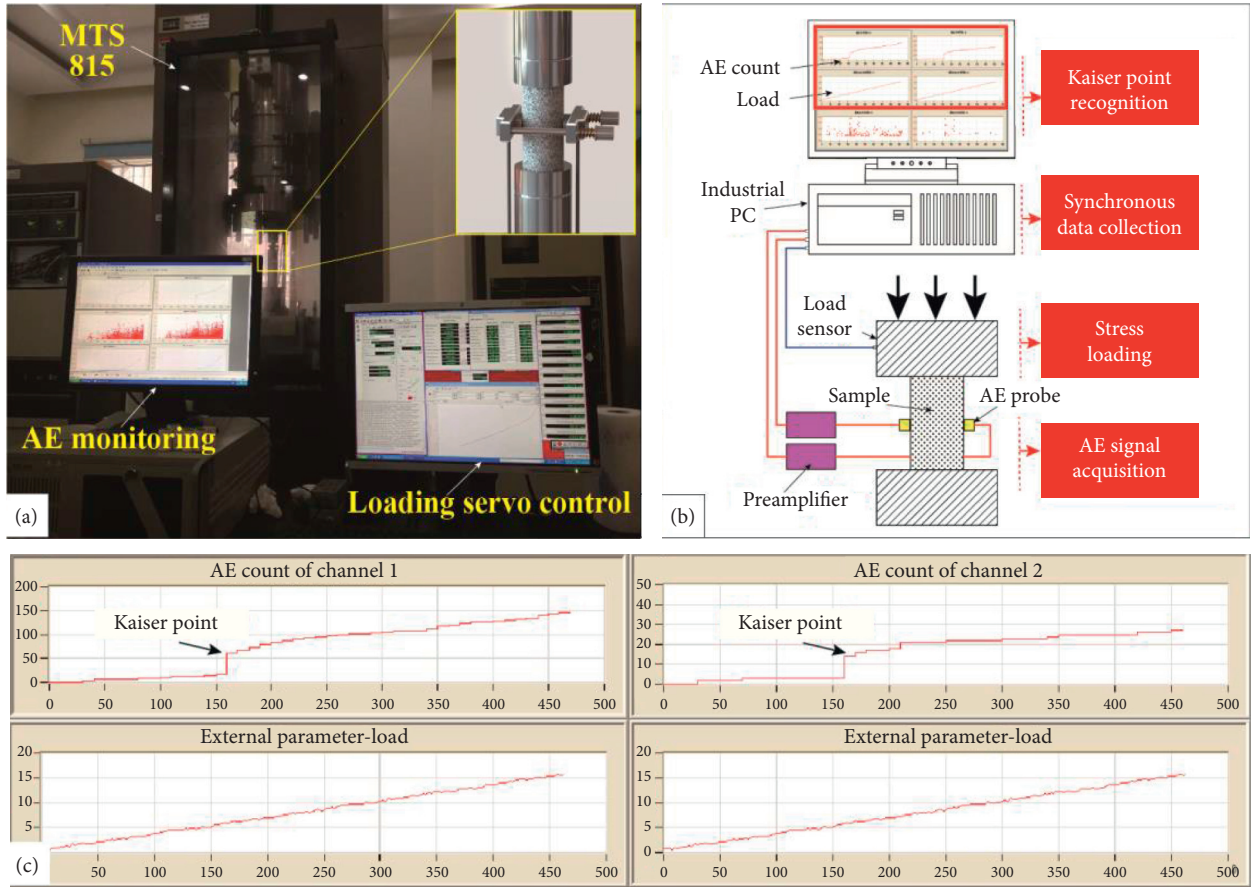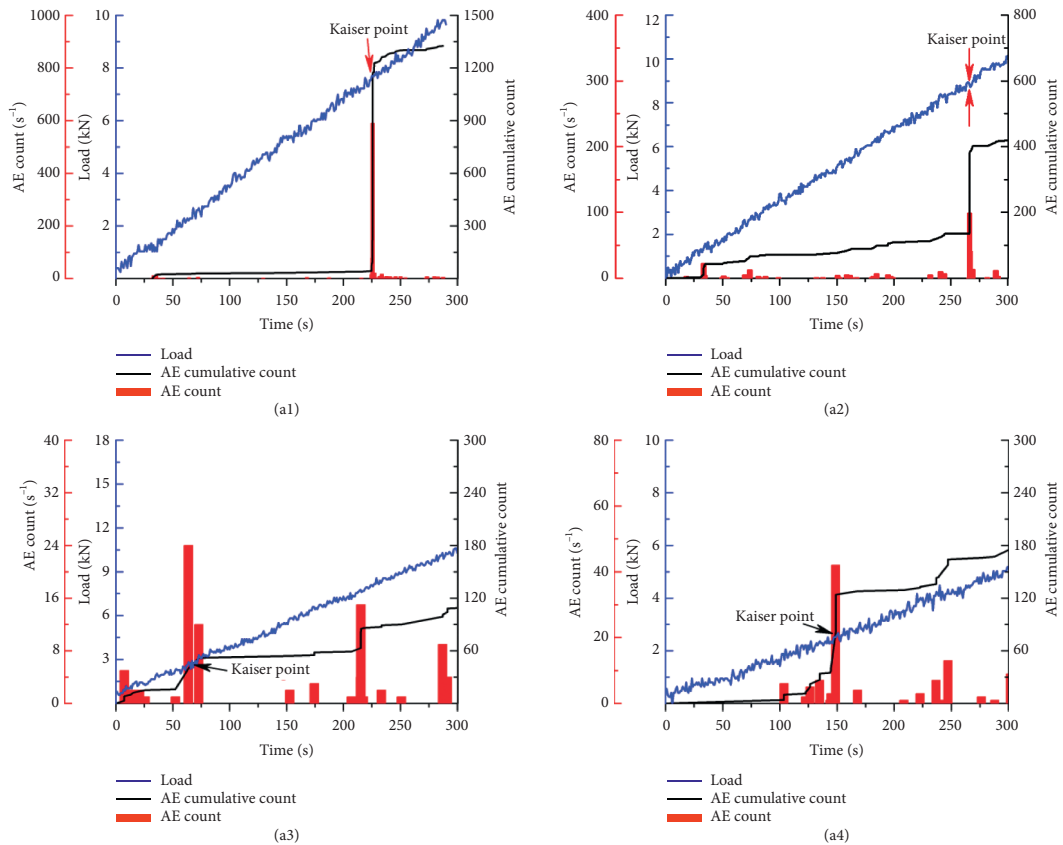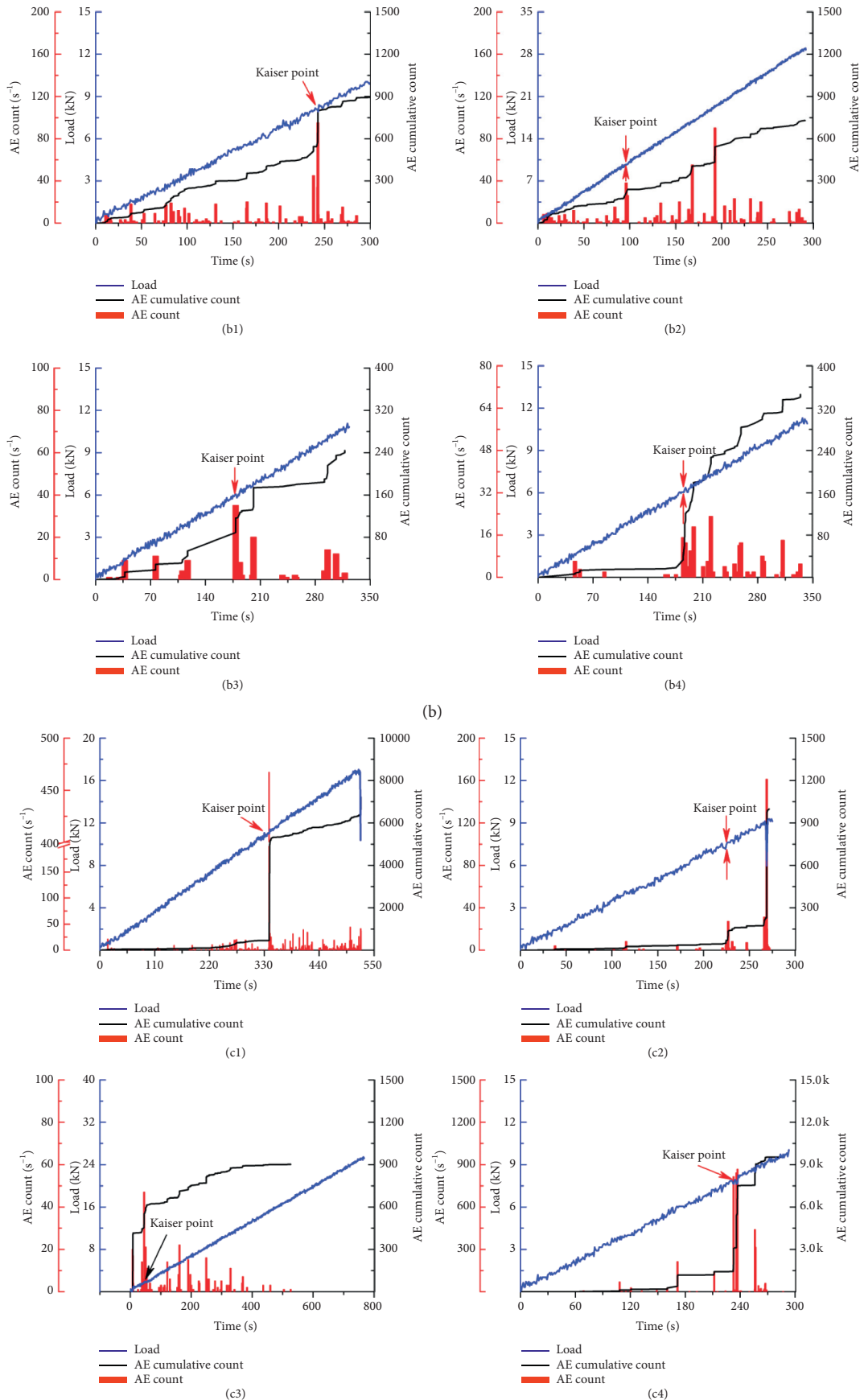
FIGURE 5: Test equipment. (a) MTS 815 material testing machine, (b) AE test schematic, and (c) identification of Kaiser point.

(a)

FIGURE 6: Continued.

(b1)

(b2)

(b3)

(b4)

(b)

(c1)

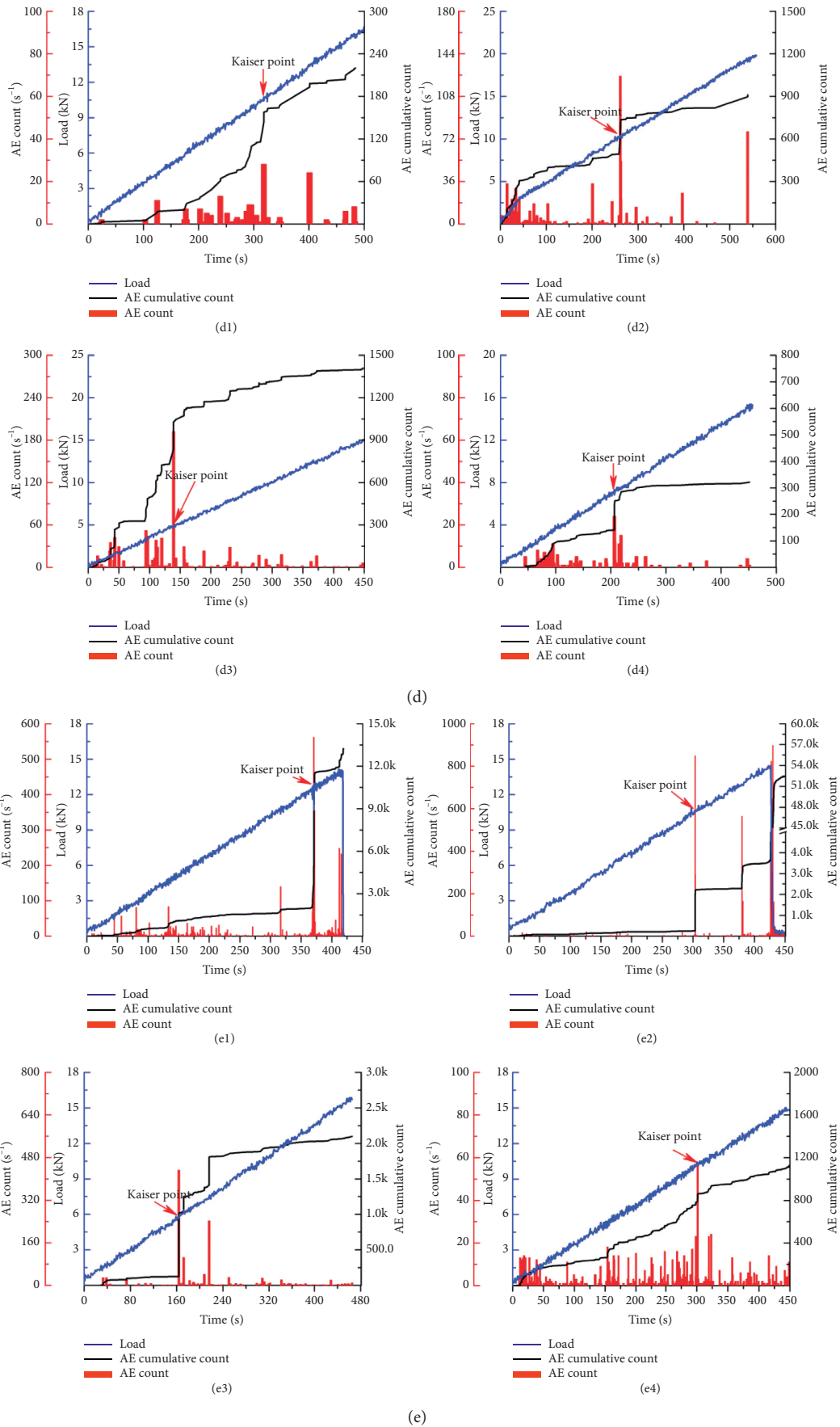(c2)

(c3)

(c4)

(c)

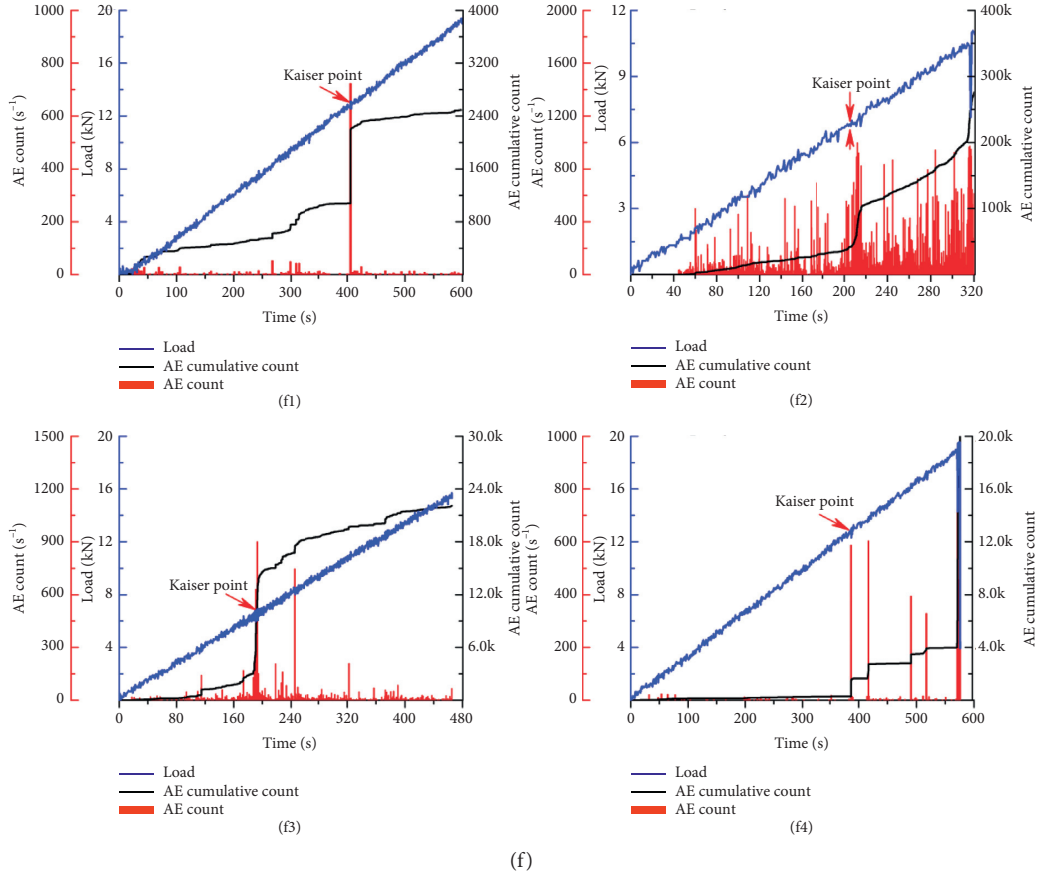FIGURE 6: Continued.

FIGURE 6: Continued.

FIGURE 6: Representative Kaiser point results at each test depth. (a1) Horizontal 0° at 200 m depth, (a2) horizontal 45° at 200 m depth, (a3) horizontal 90° at 200 m depth, (a4) vertical direction at 200 m depth, (b1) horizontal 0° at 400 m depth, (b2) horizontal 45° at 400 m depth, (b3) horizontal 90° at 400 m depth, (b4) vertical direction at 400 m depth, (c1) horizontal 0° at 600 m depth, (c2) horizontal 45° at 600 m depth, (c3) horizontal 90° at 600 m depth, (c4) vertical direction at 600 m depth, (d1) horizontal 0° at 800 m depth, (d2) horizontal 45° at 800 m depth, (d3) horizontal 90° at 800 m depth, (d4) vertical direction at 800 m depth, (e1) horizontal 0° at 900 m depth, (e2) horizontal 45° at 900 m depth, (e3) horizontal 90° at 900 m depth, (e4) vertical direction at 900 m depth, (f1) horizontal 0° at 1000 m depth, (f2) horizontal 45° at 1000 m depth, (f3) horizontal 90° at 1000 m depth, and (f4) vertical direction at 1000 m depth.

$$
\begin{cases}
\sigma_H = \dfrac{1}{2}\left(\sigma_I + \sigma_{III}\right) + \dfrac{1}{2\cos 2\beta}\left(\sigma_I - \sigma_{III}\right), \\[3mm]
\sigma_h = \dfrac{1}{2}\left(\sigma_I + \sigma_{III}\right) - \dfrac{1}{2\cos 2\beta}\left(\sigma_I - \sigma_{III}\right), \\[3mm]
\tan 2\beta = \dfrac{2\sigma_{II} - \sigma_I - \sigma_{III}}{\sigma_I - \sigma_{III}},
\end{cases}
\tag{2}
$$

where σ_I, σ_{II}, and σ_{III} are measured stresses at 0°, 45°, and 90° from clockwise direction due north, respectively; σ_H is the horizontal maximum principal stress, σ_h is the horizontal minimum principal stress, and β is the angle between the direction of horizontal maximum principal stress and the north direction, which is positive when turned counterclockwise to the north direction.

4.2. Distribution and Variation of In Situ Stress.
Figure 7(a) and Table 2 show that the in situ stress in the drilling area is dominated by horizontal tectonic stress,

especially at the borehole depth of less than 600 m. With the further increase in the depth, the dominant effect of the horizontal tectonic stress decreases, while the effect of vertical stress increases. In addition, the horizontal maximum principal stress increases with borehole depth. The horizontal minimum principal stress also increases with borehole depth, with a higher value near 400 m depth. The abnormal point of in situ stress may be related to the implicit geological structure in the local area.

The azimuth of the horizontal maximum principal stress at different depths is consistent, all of which are near the north, distributing between N5°W–N18°E, as shown in Figure 7(b).

Figure 7(c) shows that the vertical principal stress increases linearly with the borehole depth, which is consistent with the gravitational stress at the corresponding buried depth.

The linear regression analysis is performed on the stress values in Figure 7(a), and the calculation formula of the in situ stress with depth in the drilling area can be obtained:

TABLE 1: Kaiser stress of AE tests.

| Borehole depth (m) | Kaiser stress in the vertical direction (MPa) | | Kaiser stress in the horizontal direction (MPa) | | | | | |
| | | | σ_I (0°) | | σ_{II} (45°) | | σ_{III} (90°) | |
	Actual value	Average value	Actual value	Average value	Actual value	Average value	Actual value	Average value
200	5.26	5.10	13.94	18.27	18.00	16.35	4.29	5.10
	5.52		19.75		14.11		5.33	
	4.52		22.14		15.62		5.29	
	—		17.23		17.69		5.48	
400	11.09	12.35	21.72	20.02	18.73	18.71	9.44	11.96
	13.10		14.75		17.61		13.44	
	12.85		17.51		21.97		15.92	
	—		26.08		16.52		9.03	
600	16.60	16.58	25.24	22.47	16.60	13.00	4.16	5.55
	16.60		21.63		14.41		8.63	
	16.55		23.65		10.91		4.98	
	—		19.34		10.09		4.42	
800	16.61	19.91	22.61	23.06	15.54	20.15	9.41	9.73
	27.62		22.32		19.88		8.75	
	15.51		25.06		18.59		11.95	
	—		22.25		26.59		8.80	
900	17.80	23.75	30.08	24.64	20.88	21.33	11.26	11.64
	22.76		22.10		23.87		12.19	
	30.69		24.31		18.99		13.04	
	—		22.09		21.58		10.07	
1000	26.52	25.69	32.57	26.12	15.52	18.65	15.65	13.41
	21.80		24.80		17.59		10.28	
	28.76		25.30		19.49		13.40	
	—		21.80		21.99		14.33	

TABLE 2: Magnitude and direction of principal stress.

Measuring point depth (m)	Vertical principal stress σ_v (MPa)	Gravitational stress σ_G (MPa)	Horizontal maximum principal stress σ_H (MPa)	Horizontal minimum principal stress σ_h (MPa)	Horizontal maximum principal stress azimuth β (°)
200	5.10	5.50	19.75	3.62	17.66
400	12.35	11.00	20.85	11.13	17.01
600	16.58	16.50	22.53	5.49	-3.40
800	19.91	22.00	24.04	8.75	14.70
900	23.75	24.75	25.38	10.90	13.07
1000	25.69	27.50	26.22	13.31	-4.98

$$\begin{cases} \sigma_V = 0.0262h, \\ \sigma_H = 0.0082h + 17.79, \\ \sigma_h = 0.0084h + 3.38, \end{cases} \quad (3)$$

where σ_v is the predicted vertical principal stress, MPa; σ_H is the predicted horizontal maximum principal stress, MPa; σ_h is the predicted horizontal minimum principal stress, MPa; and h is the depth, m.

4.3. Comparative Verification of Measurement Accuracy.

In order to analyze the accuracy of the measured in situ stress comparatively, Xiangxi gold mine carried out verification in situ stress measurement in the underground mine with the stress relief method. The measurements were performed at a depth of 655–958 m in the mine, using the Swedish LUT rock triaxial in situ stress measurement system, as shown in Figure 8.

The magnitude and direction of the in situ stresses at the four measurement points were obtained from the LUT in situ stress calculation program, as shown in Table 3. Besides, based on the stress components obtained during stress relief, planar stress calculations were performed to solve σ_H, σ_h, and σ_v at each measurement point, as shown in Table 4. Meanwhile, (3) fitted by the AE method was also used to calculate the AE in situ stresses at the four measurement points, which were listed in Table 4 for comparative analysis.

Tables 3 and 4 show that the in situ stress measured by the stress relief method has the following distribution characteristics:
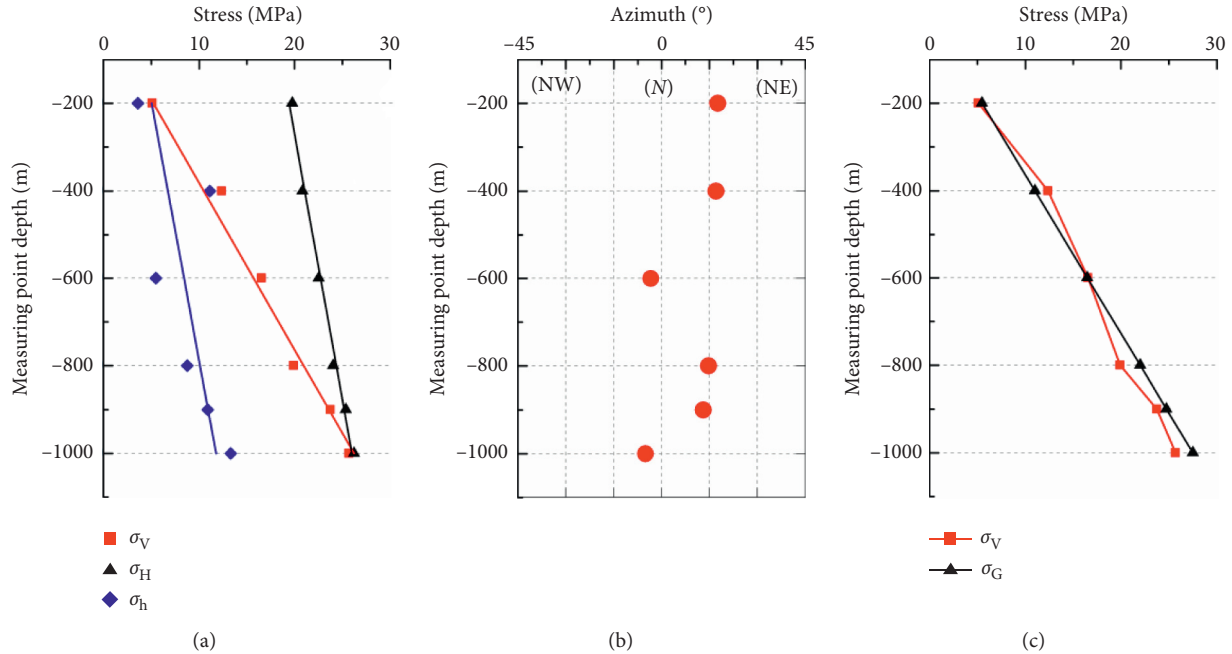
FIGURE 7: Distribution and variation of in situ stress. (a) σ_v, σ_H, and σ_h; (b) azimuth β; (c) σ_v and σ_G.
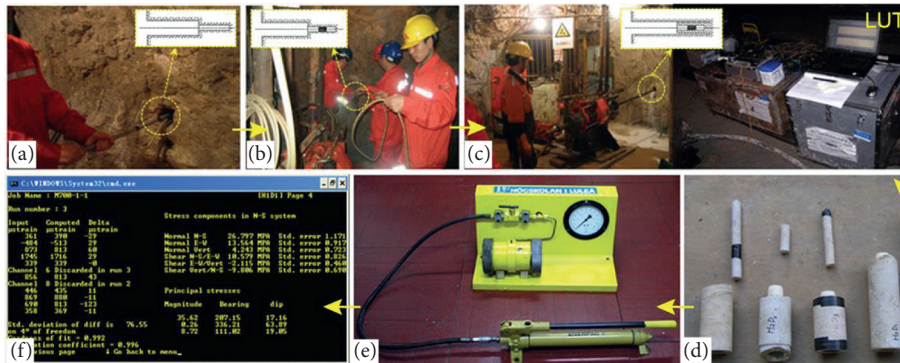

FIGURE 8: Stress relief process. (a) Drilling and cleaning, (b) installing strain gauge probe, (c) stress relief and data acquisition, (d) getting the core tube, (e) confining pressure calibration, (f) and in situ stress calculation.

(1) The dip angle of the maximum principal stress ($\sigma 1$) generally increases with depth, as shown in Table 3. The dip angle of $\sigma 1$ at a depth of 655 m is 14.17°, indicating that the $\sigma 1$ is a significant horizontal stress. When the depth increases to 756–765 m, the dip angle of $\sigma 1$ increases to 24.47°–26.91°, indicating that the $\sigma 1$ is near horizontal stress. Until the depth increases to 958 m, the dip angle of $\sigma 1$ reaches 47.34°, indicating that the $\sigma 1$ is inclined stress. The trend of dip angle of $\sigma 1$ shows that the in situ stress changes from being dominated by horizontal stress to being dominated by vertical stress with depth, which is consistent with the resulting trend of the AE method. (2) The azimuth of $\sigma 1$ is N41.16°W–N24°E, which is close to the azimuth measured

by the AE method, pointing to the near north direction, as shown in Figure 9. (3) The vertical stress (σ_V) measured by the stress relief method increases with depth, as shown in Table 4, which is also consistent with the resulting trend of the AE method.

In summary, the measurement results of the reorientation core AE method and stress relief method are in good agreement. In particular, there is consistency in the change of maximum principal stress, the azimuth of maximum principal stress, and the change of vertical stress, which shows that the reorientation core AE method is reliable. Certainly, Table 4 shows that there is some deviation in the values of σ_H, σ_h, and σ_v obtained by the two types of

TABLE 3: In situ stress results of the stress relief method.

No.	Depth (m)	Maximum principal stress σ_1			Intermediate principal stress σ_2			Minimum principal stress σ_3		
		Magnitude (MPa)	Azimuth (°)	Dip (°)	Magnitude (MPa)	Azimuth (°)	Dip (°)	Magnitude (MPa)	Azimuth (°)	Dip (°)
1#	655	29.67	24.06	14.17	11.53	285.31	31.09	2.74	135.31	55.15
2#	756	32.74	332.15	26.91	17.07	77.15	26.69	1.11	204.56	50.39
3#	765	32.27	322.84	24.47	17.67	70.18	33.22	0.58	204.04	46.62
4#	958	39.35	318.84	47.34	28.10	94.19	33.23	10.67	200.73	23.47

TABLE 4: Comparison of the results of stress relief method and AE method.

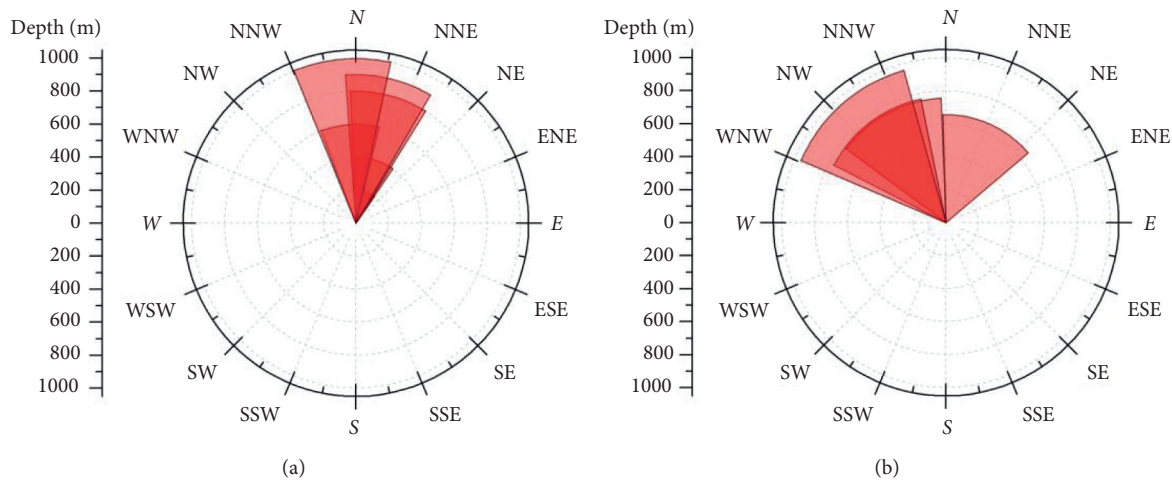| Depth	σ_H (MPa)			σ_h (MPa)			σ_v (MPa)		
	Stress relief	AE	Deviation	Stress relief	AE	Deviation	Stress relief	AE	Deviation
655	28.25	23.16	0.18	8.99	8.88	0.01	6.70	17.16	0.61
756	27.76	23.99	0.14	12.35	9.73	0.21	10.81	19.81	0.45
765	28.57	24.06	0.16	10.80	9.81	0.09	11.15	20.04	0.44
958	32.38	25.65	0.21	14.32	11.43	0.20	31.42	25.10	0.20

FIGURE 9: Azimuth of maximum principal stress. (a) Azimuth measured by AE method and (b) azimuth measured by stress relief method.

methods, which is mainly due to the difference in geological structure (shown in Figure 3) of the sampling points and the fact that the shear stresses were not taken into account in the reorientation core AE method.

5. Conclusion

In this study, an innovative deep in situ stress measurement method capable of the geological core ground reorientation technology and the AE technology was developed. With this method, the distribution of deep in situ stress of an over-kilometer-deep shaft in Xiangxi gold mine was investigated. Meanwhile, to analyze the accuracy of the measured in situ stress comparatively, the stress relief measurements were performed. The following are the conclusions drawn from this study:

(1) The geological core ground reorientation technology combines the spatial spherical geometry model and borehole bending measurement principle to reorient the geological core on an indoor calibration stage. This technology allows geological core orientation to

be separated from the drilling process without the need for in-borehole operation and has the advantages of simple operation, high accuracy, and low cost.

(2) The AE in situ stress tests were carried out with reorientation geological cores to analyze the distribution of in situ stress in deep (1040 m) borehole in the Xiangxi Gold Mine. The results show that the in situ stress changes from being dominated by horizontal stress to being dominated by vertical stress with depth. The horizontal maximum principal stress and vertical stress gradually increase with depth and reach a high-stress level (greater than 25 MPa) at a depth of 1000 m. The direction of the maximum principal stress is near north.

(3) In order to comparatively analyze the accuracy of the measured in situ stress, Xiangxi gold mine carried out verification in situ stress measurement in the underground mine with the stress relief method. The distribution of deep in situ stress obtained by the stress relief method agrees well with that by the AE

method, which proves the reliability of AE in situ stress testing method based on the geological core ground reorientation technology.

Data Availability

The data used to support the findings of this study are available from the corresponding author upon request.

Conflicts of Interest

The authors declare that they have no conflicts of interest.

Acknowledgments

References

[1] X. Ge and M. Hou, "Principle of in-situ 3D rock stress measurement with borehole wall stress relief method and its preliminary applications to determination of in-situ rock stress orientation and magnitude in Jinping hydropower station," *Science China Technological Sciences*, vol. 55, no. 4, pp. 939–949, 2012.

[2] L. J. Wang, D. S. Sun, W. R. Lin et al., "Anelastic strain recovery method to determine in-situ stress and application example," *Chinese Journal of Geophysics-Chinese Edition*, vol. 55, no. 5, pp. 1674–1681, 2012.

[3] X. Yang, J. Pang, H. Lou, and L. Fan, "Characteristics of in situ stress field at Qingshui coal mine," *International Journal of Mining Science and Technology*, vol. 25, no. 3, pp. 497–501, 2015.

[4] M. Cai and E. T. Brown, "Challenges in the mining and utilization of deep mineral resources," *Engineering*, vol. 3, no. 4, pp. 432-433, 2017.

[5] X. Li, F. Gong, M. Tao et al., "Failure mechanism and coupled static-dynamic loading theory in deep hard rock mining: a review," *Journal of Rock Mechanics and Geotechnical Engineering*, vol. 9, no. 4, pp. 767–782, 2017.

[6] H. P. Xie, F. Gao, and Y. Ju, "Research and development of rock mechanics in deep ground engineering," *Chinese Journal of Rock Mechanics and Engineering*, vol. 34, no. 11, pp. 2161–2178, 2015.

[7] X. B. Li, J. Zhou, S. F. Wang, and B. Liu, "Review and practice of deep mining for solid mineral resources," *The Chinese Journal of Nonferrous Metals*, vol. 27, no. 6, pp. 1236–1262, 2017.

[8] F.-q. Gong, Y. Luo, X.-b. Li, X.-f. Si, and M. Tao, "Experimental simulation investigation on rockburst induced by spalling failure in deep circular tunnels," *Tunnelling and Underground Space Technology*, vol. 81, pp. 413–427, 2018.

[9] F.-q. Gong, X.-f. Si, X.-b. Li, and S.-y. Wang, "Experimental investigation of strain rockburst in circular caverns under deep three-dimensional high-stress conditions," *Rock Mechanics and Rock Engineering*, vol. 52, no. 5, pp. 1459–1474, 2019.

[10] P. K. Kaiser and M. Cai, "Design of rock support system under rockburst condition," *Journal of Rock Mechanics and Geotechnical Engineering*, vol. 4, no. 3, pp. 215–227, 2012.

[11] L. R. E. Sousa, T. Miranda, R. L. E. Sousa, and J. Tinoco, "The use of data mining techniques in rockburst risk assessment," *Engineering*, vol. 3, no. 4, pp. 552–558, 2017.

[12] D. Goswami, P. Hazarika, and S. Roy, "In situ stress orientation from 3 km borehole image logs in the Koyna Seismogenic zone, Western India: implications for transitional faulting environment," *Tectonics*, vol. 39, no. 1, 17 pages, 2020.

[13] H. J. Guo, J. Ming, and W. S. Zhao, "Analysis of the distribution characteristics and laws of in situ stress in China's coal mines," *Arabian Journal of Geosciences*, vol. 13, no. 12, 14 pages, 2020.

[14] Y. Li, S. Fu, L. Qiao, Z. Liu, and Y. Zhang, "Development of twin temperature compensation and high-level biaxial pressurization calibration techniques for CSIRO in-situ stress measurement in depth," *Rock Mechanics and Rock Engineering*, vol. 52, no. 4, pp. 1115–1131, 2019.

[15] W. Yang, B. Lin, C. Zhai, X. Li, X. Sun, and C. Zhang, "A new technology for coal and gas control based on the in situ stress distribution and the roadway layout," *International Journal of Mining Science and Technology*, vol. 22, no. 2, pp. 145–149, 2012.

[16] D. Sun, W. Lin, J. Cui et al., "Three-dimensional in situ stress determination by anelastic strain recovery and its application at the Wenchuan Earthquake Fault Scientific Drilling Hole-1 (WFSD-1)," *Science China Earth Sciences*, vol. 57, no. 6, pp. 1212–1220, 2014.

[17] H. Peng, X. M. Ma, J. J. Hang, and Z. Li, "In-situ stress measurements in the WFSD-1 borehole at the Wenchuan earthquake fault," *Acta Geologica Sinica-English Edition*, vol. 89, no. 3, pp. 1049-1050, 2015.

[18] C. Zhang, M. Wu, Q. Chen, and C. Liao, "Piezomagnetic in-situ stress monitoring and its application in the Longmenshan fault zone," *Acta Geologica Sinica-English Edition*, vol. 88, no. 5, pp. 1592–1602, 2014.

[19] X. Zhao, "Application of the Kaiser effect of acoustic emission to measure vertical stress in an underground mine," *Insight-Non-destructive Testing and Condition Monitoring*, vol. 54, no. 12, pp. 662–666, 2012.

[20] J. Bai, H. Peng, X. Ma, J. Jiang, and Z. Li, "Hollow inclusion strain gauge geostress measuring instrument in deep borehole and its application example," *Chinese Journal of Rock Mechanics and Engineering*, vol. 32, no. 5, pp. 902–908, 2013.

[21] M. Hou, "Studies on new method and principle of three dimensional crustal stress measurement in deep borehole and related issues," *Chinese Journal of Rock Mechanics and Engineering*, vol. 23, no. 24, p. 5258, 2004.

[22] R. Christiansson, "The Latest Developments for In-Situ Rock Stress Measuring Techniques,", 2006.

[23] H. P. Kang, J. Lin, and X. Zhang, "Research and application of in-situ stress measurement in deep mines," *Chinese Journal of Rock Mechanics and Engineering*, vol. 26, no. 5, pp. 929–933, 2007.

[24] J. Chen, X. Li, and H. Cao, "Experimental investigation of coal-like materials for hydraulic fracturing based on fluid-solid interaction," *Journal of Natural Gas Science and Engineering*, vol. 69, 2019.

[25] D. S. Subrahmanyam, "Evaluation of hydraulic fracturing and overcoring methods to determine and compare the in situ stress parameters in porous rock mass," *Geotechnical and Geological Engineering*, vol. 37, no. 6, pp. 4777–4787, 2019.

[26] M. F. Cai, "Techniques for in-situ stress measurement at great depth," *Journal of University of Science and Technology Beijing*, vol. 11, no. 6, pp. 486–488, 2004.

[27] H. G. Li, R. Zhang, M. Z. Gao, G. Wu, and Y. F. Zhang, "Advances in technology of acoustic emission of rock," *Chinese Journal of Underground Space and Engineering*, vol. 9, no. 1, pp. 1794–1804, 2013.

[28] F. Q. Zhang, J. S. Song, Z. Y. Shen et al., "A study on fracture orientation and characteristic of remnant paleomagnetization of deep-burial volcanic rocks, north of the Songliao Basin," *Chinese Journal of Geophysics-Chinese Edition*, vol. 50, no. 4, pp. 1167–1173, 2007.

[29] Y. Lu, M. Chen, Y. Jin, W. Wu, and Y. Li, "A new method for determination of geographic orientation of deep formation geostress," *Chinese Journal of Rock Mechanics and Engineering*, vol. 30, no. 2, pp. 233–237, 2011.

[30] K. Du, X. F. Li, M. Tao, and S. F. Wang, "Experimental study on acoustic emission (AE) characteristics and crack classification during rock fracture in several basic lab tests," *International Journal of Rock Mechanics and Mining Sciences*, vol. 133, 2020.

[31] K. Peng, Z. Liu, Q. Zou, Q. Wu, and J. Zhou, "Mechanical property of granite from different buried depths under uniaxial compression and dynamic impact: an energy-based investigation," *Powder Technology*, vol. 362, pp. 729–744, 2020.